428–440 *Nucleic Acids Research, 2010, Vol. 38, No. 2* *Published online 5 November 2009*
doi:10.1093/nar/gkp844

Binding of the human nucleotide excision repair proteins XPA and XPC/HR23B to the 5*R*-thymine glycol lesion and structure of the *cis*-(5*R*,6*S*) thymine glycol epimer in the 5′-GTgG-3′ sequence: destabilization of two base pairs at the lesion site

Kyle L. Brown[1], Marina Roginskaya[2], Yue Zou[2], Alvin Altamirano[3], Ashis K. Basu[3] and Michael P. Stone[1,*]

[1]Department of Chemistry and Center in Molecular Toxicology, Vanderbilt University, Nashville, TN 37235, [2]Department of Biochemistry and Molecular Biology, James H. Quillen College of Medicine, East Tennessee State University, Johnson City, TN 37614 and [3]Department of Chemistry, University of Connecticut, Storrs, CT 06269, USA

Received September 4, 2009; Revised September 21, 2009; Accepted September 22, 2009

ABSTRACT

The 5*R* thymine glycol (5*R*-Tg) DNA lesion exists as a mixture of *cis*-(5*R*,6*S*) and *trans*-(5*R*,6*R*) epimers; these modulate base excision repair. We examine the 7:3 *cis*-(5*R*,6*S*):*trans*-(5*R*,6*R*) mixture of epimers paired opposite adenine in the 5′-GTgG-3′ sequence with regard to nucleotide excision repair. Human XPA recognizes the lesion comparably to the C8-dG acetylaminoflourene (AAF) adduct, whereas XPC/HR23B recognition of Tg is superior. 5*R*-Tg is processed by the *Escherichia coli* UvrA and UvrABC proteins less efficiently than the C8-dG AAF adduct. For the *cis*-(5*R*, 6*S*) epimer Tg and A are inserted into the helix, remaining in the Watson–Crick alignment. The Tg N3H imine and A N^6 amine protons undergo increased solvent exchange. Stacking between Tg and the 3′-neighbor G•C base pair is disrupted. The solvent accessible surface and T_2 relaxation of Tg increases. Molecular dynamics calculations predict that the axial conformation of the Tg CH_3 group is favored; propeller twisting of the Tg•A pair and hydrogen bonding between Tg OH6 and the N7 atom of the 3′-neighbor guanine alleviate steric clash with the 5′-neighbor base pair. Tg also destabilizes the 5′-neighbor G•C base pair. This may facilitate flipping both base pairs from the helix, enabling XPC/HR23B recognition prior to recruitment of XPA.

INTRODUCTION

5,6-dihydroxy-5,6-dihydro-2′-thymine, thymine glycol (Tg), is formed by exposure to radiation and chemical oxidants (1,2). It is also formed by oxidation of 5-methylcytosine to 5-methylcytosine glycol, followed by deamination (3,4). The C5 and C6 atoms of Tg are chiral and it exists in DNA as diastereomeric pairs of epimers, the 5*R* *cis*, *trans* pair (5*R*,6*S*;5*R*,6*R*) and the 5*S* *cis*, *trans* pair (5*S*,6*R*; 5*S*,6*S*) (Scheme 1) (5–7). The 5*R* pair is more abundant and more stable; in either case, the *cis* isomers predominate at the nucleoside level (6). Human cells repair hundreds of Tg lesions per day (8,9).

The 5*R*-Tg lesion has been examined in the 5′-ATgA-3′ sequence, paired opposite dA (10). It was concluded that Tg was partially extrahelical (10). It was also reported that the structure of 5*R*-Tg placed opposite dA in the 5′-GTgC-3′ sequence was disordered (11). These studies (10,11) did not report *cis–trans* epimerization (5–7) of Tg. In DNA the complementary base modulates the *cis–trans* equilibrium of 5*R*-Tg. When paired opposite dA in the 5′-GTgG-3′ sequence a 7:3 *cis* (5*R*,6*S*): *trans* (5*R*,6*R*) mixture exists at equilibrium at 25°C, whereas

*To whom correspondence should be addressed. Tel: +1 615 322 2589; Fax: +1 615 322 7591; Email: michael.p.stone@vanderbilt.edu

The authors wish it to be known that, in their opinion, the first two authors should be regarded as joint First Authors.

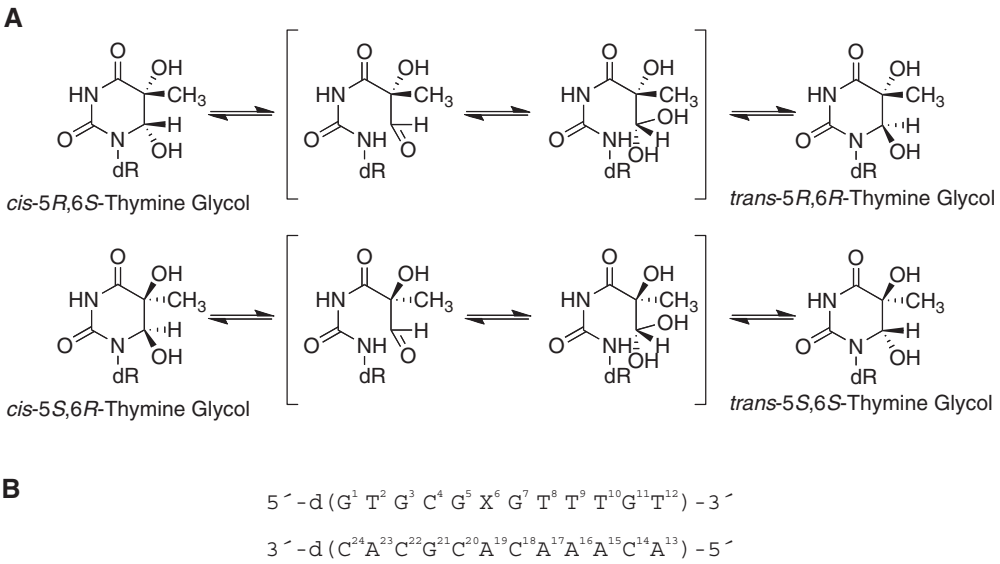

Scheme 1. (**A**) Interconversion of the *cis*-(5*R*,6*S*) and *trans*-(5*R*,6*R*) Tg lesions. When the 5*R*-Tg isomer is paired opposite dA in this 5′-GTgG-3′ sequence a 7:3 *cis*-(5*R*,6*S*): *trans*-(5*R*,6*R*) mixture is present at equilibrium, in slow exchange on the NMR timescale (12). (**B**) Oligodeoxynucleotide duplex used for NMR studies, indicating the numbering of the nucleotides. X^6 is the *cis*-(5*R*,6*S*) Tg lesion.

when paired with dG in the same sequence, only the *cis* (5*R*,6*S*) epimer is observed (12). When *cis*-(5*R*,6*S*) Tg is mismatched with dG in the 5′-GTgG-3′ sequence it assumes the wobble orientation, and shifts toward the major groove. This increases its solvent accessible surface but it remains stacked into the helix. Intrastrand hydrogen bonding between the hydroxyl on C6 of Tg and the N7 of the 3′ purine (13) is weak (14).

The 5*R*-Tg lesion hinders DNA replication (15,16). It is a substrate for base excision repair. This is mediated by at least two DNA *N*-glycosylase/AP lyases that are influenced by the diastereoisomer of Tg, the *cis–trans* epimerization of each diastereoisomer, and the identity of the complementary purine (17). The 5*R*-Tg lesion is also repaired by nucleotide excision repair (NER), although the effects of the *cis–trans* epimerization of each diastereoisomer of Tg with regard to NER have not been characterized. Both randomly introduced 5*R*-Tg and abasic sites are substrates for the *Escherichia coli* UvrABC proteins (18,19). Tg is also excised *in vitro* by human NER (20).

Here we report on the 7:3 *cis*-(5*R*,6*S*):*trans*-(5*R*,6*R*) mixture of Tg epimers paired opposite adenine in the 5′-GTgG-3′ sequence (12) with regard to NER by the NER proteins of *E. coli* and the binding of the lesion by the human NER proteins XPA and XPC/HR23B. The 5*R*-Tg lesion is a good substrate for binding by UvrA and excision by UvrABC, although the bulky C8-dG DNA adduct of AAF is recognized and incised more efficiently. However, recognition of 5*R*-Tg by the human XPC/HR23B complex is superior to the bulky AAF adduct, whereas recognition by human XPA is comparable to the AAF adduct. To elucidate structure–activity relationships underlying these observations, the structure of the *cis*-(5*R*,6*S*) Tg epimer embedded in the same 5′-GTgG-3′ sequence and placed opposite to deoxyadenosine has also been refined. It remains in the Watson–Crick orientation with respect to the complementary dA, but the solvent accessible surface area of Tg is increased. The complementary A^{19} remains stacked in the helix. Significantly, the 5*R*-Tg lesion also destabilizes the 5′-neighbor G•C base pair. We propose that this lowers the activation barrier with respect to flipping both base pairs from the helix, at least in this particular sequence, enabling XPC/HR23B to recognize 5*R*-Tg prior to the recruitment of XPA.

METHODS

Sample preparation

The undamaged ND-50-bp and AAF-50-bp oligodeoxynucleotides were constructed as described (21). The Tg-modified 5′-d(GTGCGTgGTTTGT)-3′ (17) was characterized using a Voyager-DE MALDI-TOF mass spectrometer (PerSeptive Biosystems, Inc., Foster City, CA, USA). It was ligated with a 5′-^{32}P-labeled 20-mer, and a 19-mer on the 5′- and 3′-ends, respectively, to form the 5′-^{32}P-labeled Tg-51mer. The oligodeoxynucleotides 5′-d(GTGCGTGTTTGT)-3′ and 5′-d(ACAAACAC GCAC)-3′ were purchased from the Midland Certified Reagent Co. (Midland, TX, USA) and purified by reverse phase HPLC.

Binding as measured by electrophoretic mobility shift assays

Assays for the UvrA protein were performed as described (21). For the human NER proteins XPA and XPC/HR23B, the binding assay was performed as described for XPA binding (22), with minor modifications. The radioactivity of DNA bands on gels was quantified using a Fuji FLA-5000 phosphoimager. Dissociation constants

(K_d) were determined from the binding curves as a concentration of the substrate at which half of DNA was bound to protein. Three experiments were performed for each binding curve.

UVrABC incision assays

The 5′-^{32}P-labeled substrates (2 nM) were incised by UvrABC nucleases (UvrA, 15 nM; UvrB, 250 nM; UvrC, 100 nM) in the UvrABC buffer with 1 mM ATP at 37°C and the products were resolved on a 12% polyacrylamide gel and analyzed as described (21). The initial rates were calculated by linear least-squares fits of data. The substrate incised in femtomoles was calculated based on the total molar amount of substrate employed in each reaction and the incision percentage of the substrate. Three experiments were performed to determine initial rates.

Nuclear magnetic resonance spectroscopy

Oligodeoxynucleotides were annealed in 20 mM sodium phosphate, containing 100 mM NaCl, 10 μM NaN_3 and 50 μM Na_2EDTA (pH 7.0). Experiments were performed at 800 MHz. NOESY spectra for the nonexchangeable protons were recorded at 30°C with mixing times of 80, 150, 200 and 250 ms using States-TPPI phase cycling, 512 real data points in the d1 dimension with 32 scans per FID, 2K real data points in the d2 dimension, sweep width of 10 p.p.m., and a relaxation delay of 2.0 s. The water resonance was suppressed using presaturation. NOESY spectra of exchangeable protons were obtained at 5°C using watergate H_2O suppression (23). T_1 spin–lattice relaxation experiments were collected using the inversion recovery method (24,25). T_2 transverse relaxation experiments were collected using the CPMG method (24,25). ^{1}H spectra were referenced to 3-(trimethylsilyl)propionic-2,2,3,3-d_4 acid, sodium salt (3-TMSP). The program XWINNMR (Bruker Inc., Billerica, MA, USA) was used for data processing. A skewed sinebell-squared apodization function with a 90° phase shift was used for NOESY experiments; the same function with a 10° phase shift was used for COSY experiments.

Distance restraints

NOE intensities were determined from volume integration using SPARKY (26). Intensities for the *cis*-(5*R*, 6*S*) epimer were corrected for the 7:3 *cis*-(5*R*,6*S*):*trans*-(5*R*,6*R*) molar ratio. These were combined with intensities generated from CORMA analysis of a B-form starting structure producing a hybrid intensity matrix (27,28), which was refined using MARDIGRAS (29–31) with the RANDMARDI function. Calculations at mixing times of 80, 150, 200 and 250 ms were run at correlation times of 2, 3, 4 and 5 ns. Distance restraints were divided into categories indicative of confidence levels. Empirical restraints were used to define Watson–Crick hydrogen bonding, but not for the Tg ^{6}•A^{19} or G^5•C^{20} pairs.

Torsion angle restraints

^3J ^{1}H coupling constants were obtained by amplitude constrained multiplet evaluation of COSY data (32). Electronegativity of substituent Karplus curves were generated and converted to phase angle space assuming a maximum pucker amplitude (Φ) of 44° (33,34). Scalar couplings were fit to the curves to determine pseudorotation ranges (*P*). The sugar pseudorotation and amplitude ranges were converted to restraints for the dihedral angles ν_0 to ν_4. Measurements of the mol fraction of sugar puckers in the N or S conformations were determined from the sum of $J_{1'2'}$ and $J_{1'2''}$ scalar couplings (34). Nucleotides with <50% X_S were allowed to explore both N and S conformations during rMD calculations (ρ = 0°–210°). Nucleotides with X_S > 50% were restrained such that ρ = 125°–210°. Backbone torsion angles were restrained with data where available; otherwise they were restrained empirically based on canonical A-form and B-form values.

Structural refinement

Partial charges for Tg were generated using GAUSSIAN (35). Geometry optimization and ESP calculations were performed using the Hartree–Fock method with the 6-31G* basis set (12). The output was formatted using ANTECHAMBER (36). Starting structures were generated using NAB (37) and energy minimized using the SANDER module of AMBER (36). Coordinate and topology files were generated with xLEaP (36) using ff99 parameters (38). The restraint function utilized square-well potentials (39). The generalized Born model was used for simulated annealing calculations, with a salt concentration of 0.2 mM (40,41). Temperature was maintained using the Berendsen algorithm (42). Complete relaxation matrix analysis (27,28) was performed to determine agreement with ^{1}H NOESY data. A refined structure from simulated annealing was neutralized with the addition of sodium ions and placed in a truncated octahedral TIP3P water box with periodic boundaries at a distance of 8 Å from the solute. After equilibration, a 10-ns isothermal rMD calculation was performed. The temperature was controlled using the Langevin thermostat (43,44) with a collision frequency of 1 ps^{-1}. Electrostatic interactions were treated with the PME method (45). A 15-Å cutoff for nonbonded interactions was used. Bond lengths involving hydrogen were fixed using SHAKE (46). A structural ensemble was extracted from the isothermal trajectory using PTRAJ (36). The heavy atoms were subjected to pairwise RMSD comparisons using SUPPOSE. Helicoidal analysis was performed using CURVES (47,48). Structures were rendered using Chimera (49). Solvent-excluded and solvent-accessible surface areas of individual bases as a function of probe radius were calculated using MSMS (50).

RESULTS

Dodecamer containing the 5*R*-Tg lesion

The 5′-d(GTGCGXGTTTGT)-3′, X = 5*R*-Tg, was subjected to mass spectrometric analysis, which yielded the anticipated molecular ion peak with mass 3732 (m/z). Capillary gel electrophoretic and HPLC analysis showed that it eluted as a single peak. The adducted

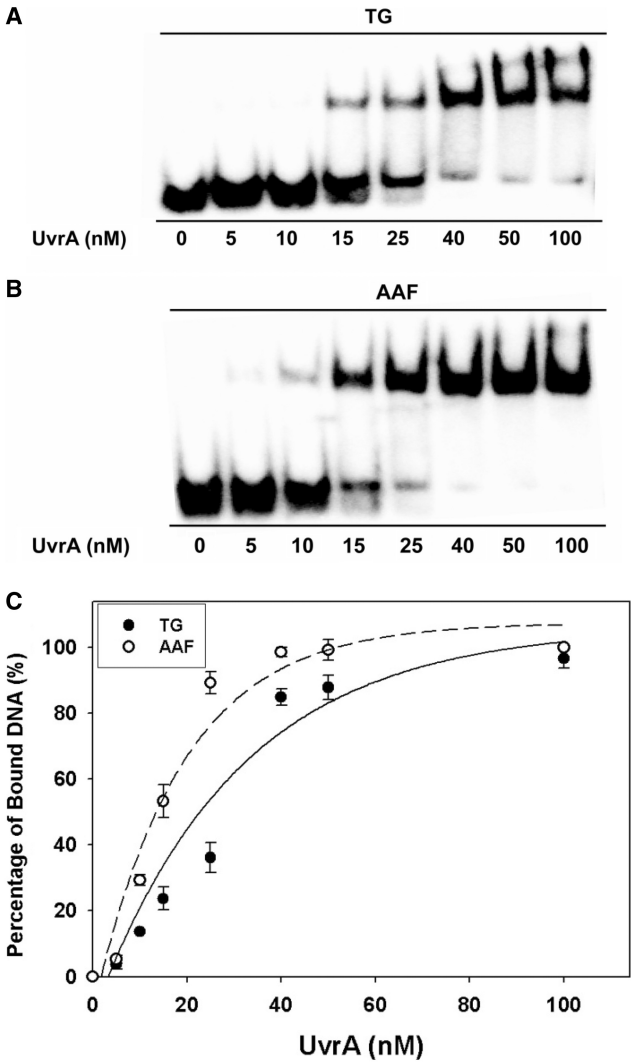

Figure 1. Binding of UvrA to the duplex containing the site-specific 5*R*-Tg lesion paired with dA. In (**A**) and (**B**), UvrA at the indicated concentrations was incubated with 2-nM substrates at 37°C for 20 min in UvrABC binding buffer and then analyzed on a 3.5% polyacrylamide native gel by gel mobility shift assays. (A) TG-51 bp; (B) AAF-50 bp. (**C**) The binding curves generated based on the titration data in (A) and (B).

oligodeoxynucleotide was pure and existed as a single chromatographically separable species.

Recognition and incision of the 5*R*-Tg substrate by *E. coli* UvrABC proteins

A 51-bp substrate containing 5*R*-Tg (Supplementary Scheme S1) was utilized. A 50-bp substrate containing an AAF adduct (AAF-50 bp) that is recognized and incised by *E. coli* UvrABC (21), was used for comparison. A 50-bp substrate (ND-50 bp) was used as a negative control. Figure 1A and B show gel mobility shift assays for UvrA binding to Tg and AAF substrates, respectively. The slowly migrating bands represent the formation of DNA–$UvrA_2$ complexes. Binding isotherms (Figure 1C) showed that the affinity of UvrA to the 5*R*-Tg substrate was high, though the binding of UvrA to the AAF substrate was stronger (Table 1). The UvrA had a 2.4-fold lower affinity to the Tg-50-bp substrate ($K_d = 24 \pm 2$ nM) than the AAF-51-bp substrate ($K_d = 10 \pm 1$ nM). The K_d for UvrA binding to the AAF substrate agreed with the reported value (21). UvrA had lower affinity to the undamaged than to the damaged substrate, in agreement with previous observations (21). While the differing sequence contexts of the Tg- and AAF–DNA substrates (Scheme 2A) might affect their interactions with the UvrABC system (51–53), it was assumed that sequence specific effects were smaller than those caused by the difference in the types of DNA lesions.

Table 1. Equilibrium dissociation constants for binding of UvrA and human NER proteins to TG-51-bp and AAF-50-bp DNA substrates at 30°C[a]

Protein	K_d for TG-51 bp (nM)	K_d for AAF-50 bp (nM)
UvrA	24 ± 2	10 ± 1
XPA[b]	48 ± 4	44 ± 6
XPC/HR23B	18 ± 2	27 ± 3

[a]Data represent the means ± SD of three experiments.
[b]For XPA the dissociation constants were determined for XPA dimers.

UvrC cut the damaged strand 4 or 5 nt 3′ to the lesion and then 8 nt 5′ to the lesion (Supplementary Scheme S1). The substrates were ^{32}P-labeled at the 5′-end and the incision products of were 18-mers. Figure 2A and B show temporal data for UvrABC incision of Tg and AAF substrates, respectively. No products were observed for the ND-50-bp undamaged substrate. The initial rates were determined from the relative yields of the products (Figure 2C). For the 5R-Tg substrate the initial rate was 0.48 ± 0.04 fmol/min. For the AAF substrate the comparable rate was 0.80 ± 0.02 fmol/min. Thus, the 5*R*-Tg substrate was incised 1.7X less efficiently than was the AAF substrate. However, the incision rate of the 5*R*-Tg substrate was greater than that of the DNA helix-distorting cross-linked tandem G(8,5-Me)T lesion (21). Therefore, in this sequence 5*R*-Tg was a good substrate for the *E. coli* UvrABC proteins. The ratio of binding affinities of UvrA to the AAF- versus 5*R*-Tg substrate was 2.4, greater than the ratio of initial rates of UvrABC incision of the AAF- and 5*R*-Tg substrates, which was 1.7.

Binding of human NER proteins to the 5*R*-Tg substrate

The binding of XPA and XPC/HR23B to the 5*R*-Tg damaged duplex was compared with the AAF-damaged duplex using EMSA (Figure 3). Neither XPA nor XPC/HR23B bound to the undamaged substrate. The shifted bands represent formation of DNA–XPA_2 complexes. At low concentrations XPA bound to AAF-50 bp with a greater affinity than to Tg-51 bp, which was evident from a comparison of the 25 nM XPA lanes for 5*R*-Tg and AAF. At concentrations >50 nM, XPA bound to both substrates with comparable affinities (Figure 3A). The binding of XPC/HR23B to 5*R*-Tg and AAF-damaged

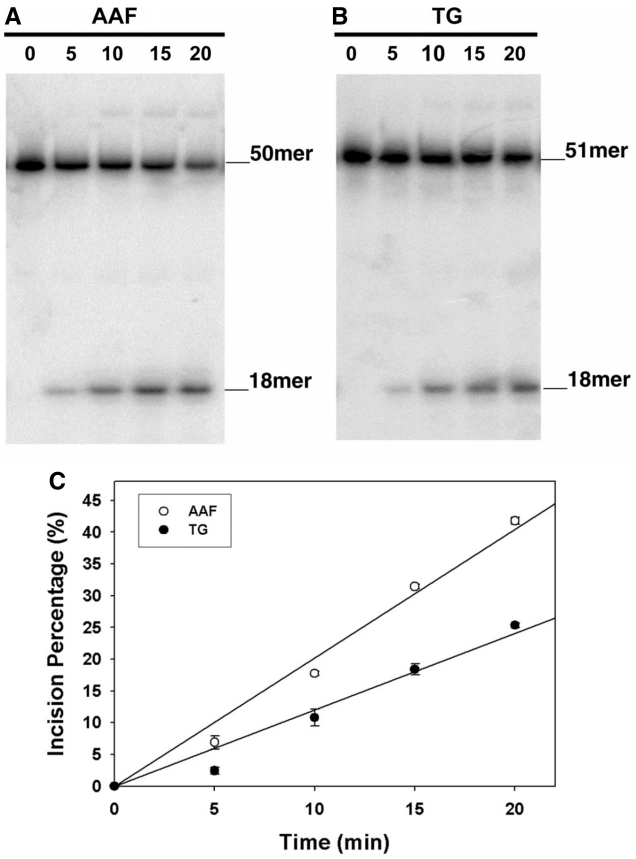

Figure 2. Incisions of the site-specific 5*R*-Tg paired with dA substrate by UvrABC nuclease. In (**A**) and (**B**), 2-nM DNA substrates 5′-terminally labeled with ^{32}P were incubated with UvrABC proteins in the UvrABC buffer in the presence of 1-mM ATP at 37°C for the indicated time periods. The incision products were analyzed on a 12% urea PAGE under denaturing conditions. (A) AAF-50 bp; (B) Tg-51 bp. (**C**) Kinetics of UvrABC incisions based upon the data in (A) and (B).

DNA is shown in Figure 3B. Figure 3C shows binding isotherms for XPA interacting with the 5*R*-Tg- and AAF–DNA substrates. The dissociation constants estimated for the 5*R*-Tg and AAF substrates were similar, 48 ± 4 nM and 44 ± 6 nM, respectively (Table 1). XPC/HR23B bound to Tg-51 bp with a greater affinity than to AAF-50 bp (Figure 3D). Unlike XPC/HR23B the *E. coli* NER protein UvrA bound better to AAF–DNA adduct than to Tg-DNA adduct (Figure 1).

Nuclear magnetic resonance spectroscopy

Data were collected upon preparation of the duplex containing the 5*R*-Tg lesion (Scheme 1), and again after 4 weeks. Spectral changes were not observed, suggesting that the *cis*-(5*R*,6*S*) and *trans*-(5*R*,6*R*) epimers had achieved equilibrium. The *cis*-(5*R*,6*S*) epimer was favored 7:3 over the *trans*-(5*R*,6*R*) epimer, as determined by integration of Tg CH_3 peaks (12). It was possible to obtain spectroscopic data for the *cis*-(5*R*,6*S*) epimer; the *trans*-(5*R*,6*R*) epimer was not present at sufficient levels to allow evaluation of its spectrum.

Nonexchangeable DNA protons. Figure S1 in the Supplementary Data shows NOESY cross-peaks between the base aromatic H6/H8 protons and the deoxyribose H1′ protons. The resonances were assigned using standard strategies (54,55). Complete sequential NOE connectivity was obtained for both the modified and the complementary strands. With the exception of several of the H4′ protons, and the stereotopic assignments of the H5′ and H5″ sugar protons, assignments of the deoxyribose protons were made unequivocally; the resonance assignments have been reported (12).

Exchangeable DNA protons. Supplementary Figure S2 shows NOESY cross-peaks between the purine N1H and pyrimidine N3H imino protons and the amino protons of the complementary bases, involved in Watson–Crick hydrogen bonding. At the mismatched X^6•A^{19} pair, the Tg N3H imino resonance was not identified. This was attributed to rapid exchange with solvent. The assignments of the remaining hydrogen-bonded imino and amino protons were made using standard methods (56). The G^5 N1H imino resonance was broad at 5°C and disappeared when the temperature was increased to 15°C. In contrast, for an unmodified duplex, the G^5 N1H imino resonance was sharp and was observed at temperatures as high as 40°C (12). There was no cross peak between the G^5 N1H resonance and G^{21} N1H, located at base pair C^4•G^{21}. This was attributed to its exchange with solvent. The imino resonances for base pairs T^2•A^{23}, G^3•C^{22}, C^4•G^{21}, G^7•C^{18}, T^8•A^{17}, T^9•A^{16}, T^{10}•A^{15} and G^{11}•C^{14} were observed. The imino resonances for the terminal base pairs G^1•C^{24} and T^{12}•A^{13} were not observed, attributed to exchange broadening with water. The assignments have been reported (12).

Tg protons. Figure 4 shows NOESY data obtained for the Tg CH_3 and Tg H6 protons. The proximate Tg H6 and Tg CH_3 protons yielded a strong Tg H6→Tg CH_3 NOE at all mixing times. The G^5 H1′→X^6 H6 and G^5 H8→X^6 H6 NOEs were diagnostic of the *cis*-(5*R*,6*S*) configuration. The *cis*-(5*R*,6*S*) Tg CH_3 protons exhibited a chemical shift of 0.49 p.p.m., while the Tg H6 proton resonated at 4.58 p.p.m. A total of 23 NOE cross peaks were assigned between Tg CH_3 and H6 in the *cis*-(5*R*,6*S*) epimer and DNA (seven for Tg H6 and sixteen for Tg CH_3). The *trans*-(5*R*,6*R*) Tg CH_3 protons exhibited a chemical shift of 1.24 p.p.m., while the Tg H6 proton resonated at 4.91 p.p.m. For the *trans*-(5*R*,6*R*) epimer, only one NOE cross peak was observed, between Tg H6 and Tg H2′. Integration of the respective Tg H6→Tg H2′ cross peaks confirmed the 7:3 ratio of epimers. A single set of resonances was observed for G^5 and G^7. Thus, the equilibrium mixture of epimers did not influence the chemical shift environment of the neighboring nucleotides. The spectroscopic assignments have been reported (12).

Spin–lattice relaxation

The T_1 relaxation times of the T^2, T^8, T^9, T^{10}, & T^{12} CH_3 and X^6 CH_3 groups were compared to those of the unmodified duplex (Supplementary Figure S3). The X^6

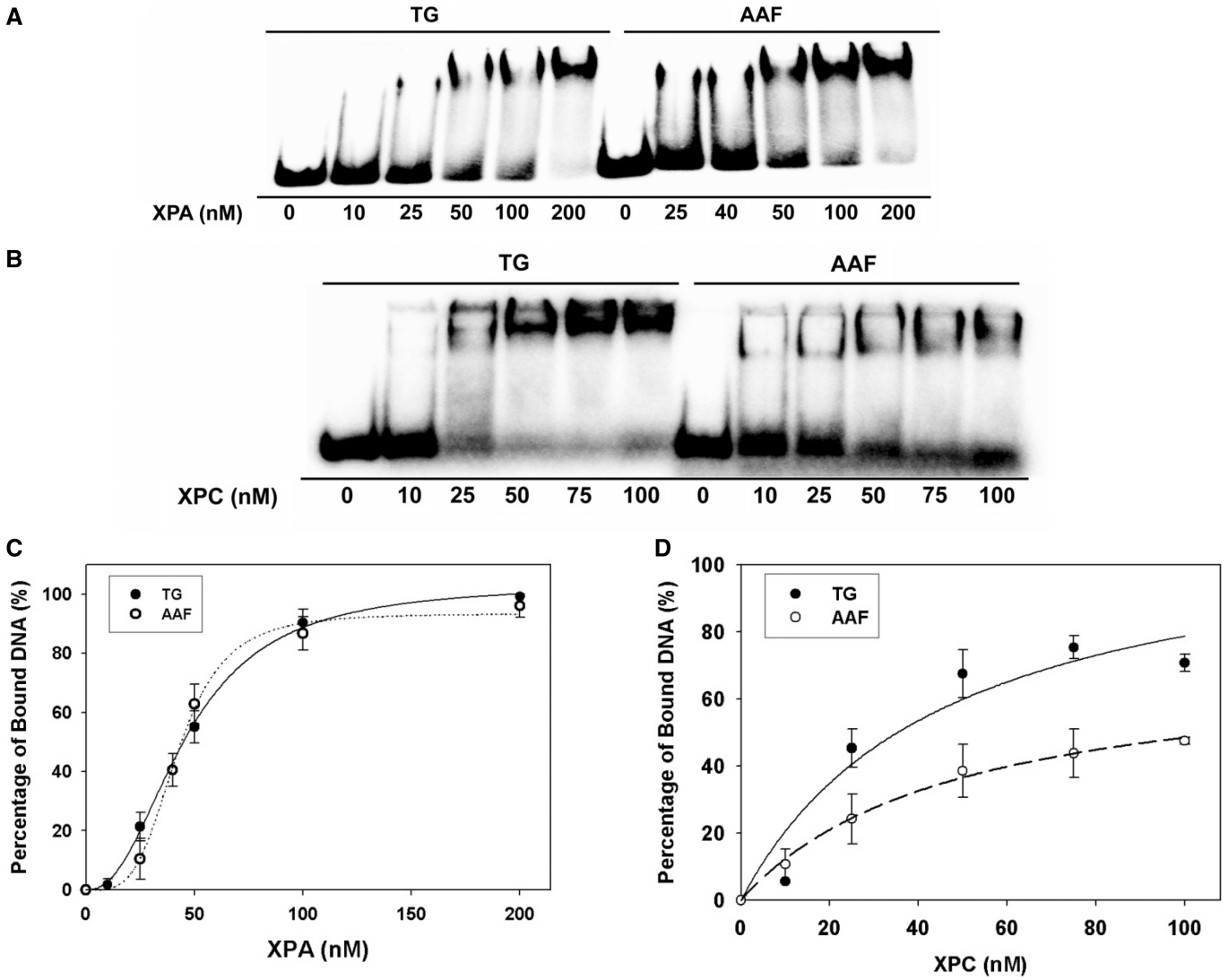

Figure 3. Binding of human XPC/HR23B and XPA proteins to the site-specific 5*R*-Tg paired with dA substrate. In (**A**) and (**B**), XPA (A) or XPC/HR23B (B) proteins at the indicated concentrations were incubated with 4-nM substrates at 30°C for 30 min in XPA binding buffer and then analyzed on 3.5% polyacrylamide native gels by gel mobility shift assays (XPA, 4°C; XPC/HR23B, room temperature). (**C**) and (**D**) show the binding curves generated from the data in (**A**) and (**B**).

CH_3 T_1 relaxation time was 1.9 s faster than was the corresponding T^6 CH_3 relaxation time of the unmodified duplex containing $T^6 \bullet A^{19}$. The X^6 CH_3 relaxed an average of 1.4 s faster than other thymine CH_3 groups in the $X^6 \bullet A^{19}$ duplex.

Spin–spin relaxation

The T_2 relaxation times of the T^2, T^8, T^9, T^{10}, & T^{12} CH_3 and X^6 CH_3 groups were compared to those of the unmodified duplex (Supplementary Figure S4). The Tg CH_3 of the $X^6 \bullet A^{19}$ duplex relaxed ~70 ms faster than the corresponding CH_3 of the unmodified sample.

Structural refinement

Thirty starting structures were generated, of which half had the Tg CH_3 group in the axial conformation and half had the Tg CH_3 group in the equatorial conformation. These exhibited a maximum pairwise RMSD of 4.3 Å. The distance and torsion angle restraints used in the calculations are summarized in Supplementary Table S1. As Watson–Crick hydrogen bonding at the $X^6 \bullet A^{19}$ base pair was not observed, hydrogen bond restraints between X^6 and A^{19} were not used. All but three of the 30 structures emerged from simulated annealing calculations with Tg CH_3 in the axial conformation. A refined structure with Tg CH_3 in the axial conformation was placed into a truncated octahedron TIP3P water box, and subjected to 10 ns of isothermal rMD calculations at 300 K (Supplementary Figure S5). At 4.38 ns the Tg CH_3–C5–C6–H6 torsion angle shifted from −40° to 50°. This corresponded to a change from the Tg CH_3 axial to the equatorial conformation. The glycosyl Tg O4′–H1′–N1–C2 torsion angle fluctuated between −90° and −140°

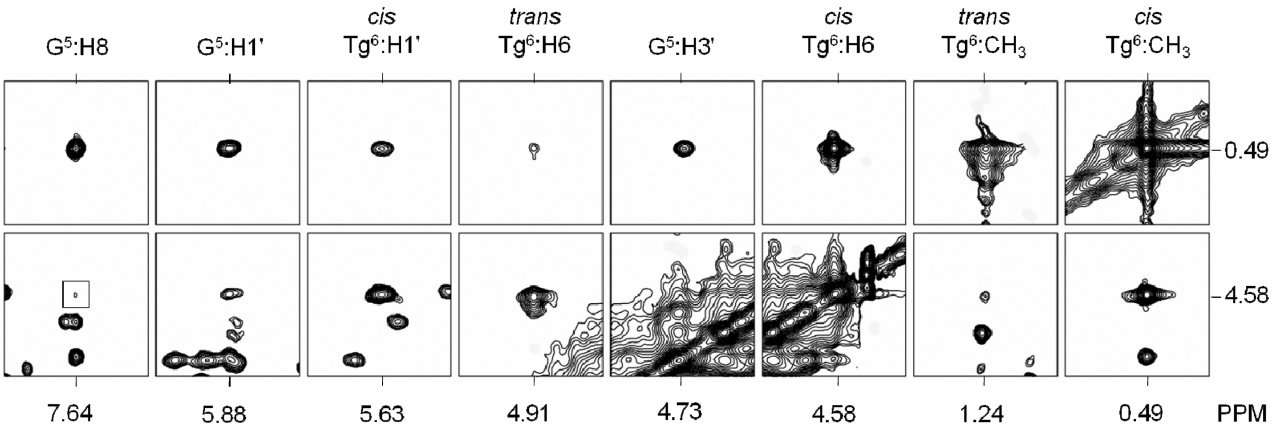

Figure 4. (**A**) NOESY data collected at a NOE mixing time of 250 ms, showing NOEs between the *cis*-(5*R*,6*S*) Tg lesion and the DNA that were used for structural refinement. The spectra were collected at 800 MHz at a temperature of 30°C.

during the first 4.38 ns; when the Tg CH_3 group shifted from axial to equatorial conformation, this angle fluctuated between −130° and −150°.

The distances between Tg HO5→G^7 N7 (Supplementary Figure S5, panel C) and Tg HO6→G^7 N7 (Supplementary Figure S5, panel D) were monitored during the isothermal calculations. Analysis of trajectories indicated intra-strand hydrogen bond stabilization of the X^6•A^{19} base pair as predicted (13). Hydrogen bond occupancy was defined as hydrogen bond donors and acceptors being within 3.5 Å with an angle cutoff of 120°. During the first 4.38 ns, in which the Tg CH_3 group was in the axial conformation, the Tg HO6→G^7 N7 hydrogen bond criteria were satisfied (Supplementary Figure S5, panel D). This induced altered propeller twist at the lesion site. There was 42% occupancy of the Tg OH6→G^7 N7 hydrogen bond during the trajectory and the entirety of this occupancy occurred during the first 4.38 ns. In contrast, during the first 4.38 ns, in which the Tg CH_3 group was in the axial conformation, the distance between Tg HO5 and G^7 N7 was 4.5 Å, which was not consistent with hydrogen bonding. As a consequence of Tg CH_3 reorienting to the equatorial conformation at 4.38 ns, Tg OH5 shifted to the axial conformation. This allowed for hydrogen bond formation with G^7 N7. The Tg OH5→G^7 N7 occupancy was 11% over 10 ns and was only observed after the conformational shift. During these isothermal calculations, the RMSD of the DNA backbone heavy atoms (Supplementary Figure S5, panel F) was 2 Å.

Structural ensembles representing both axial and equatorial conformations of Tg CH_3 were extracted for analyses (Supplementary Figure S6). The axial ensemble (PDB ID 2KH5) was extracted from the 120 ps before the conformation change at 4.38 ns; this ensemble had an RMSD of 0.56 Å for the core 6 bp. The equatorial ensemble (PDB ID 2KH6) was extracted 1 ns after the conformational change at 4.38 ns. This had an RMSD of 0.69 Å for the core 6 bp.

To evaluate the accuracies of the rMD ensembles with respect to the ^{1}H NOESY data, complete relaxation matrix analyses (27,28) were performed (Supplementary Figure S7). The ensemble with Tg CH_3 in the axial conformation had an average sixth root residual R_1^X value of 8.12×10^{-2}. The Tg lesion exhibited an R_1^X value of 7.19×10^{-2} for inter-nucleotide cross-peaks with G^5 and 7.61×10^{-2} for intra-nucleotide cross-peaks. The ensemble with Tg CH_3 in the equatorial position had an average R_1^X value of 8.15×10^{-2}. The Tg lesion exhibited an R_1^X value of 1.77×10^{-1} for inter-nucleotide cross peaks with G^5 and 1.01×10^{-1} for intra-nucleotide cross-peaks. This indicated that both ensembles of structures satisfied the ^{1}H NOESY data, although at the lesion site, the agreement between the structures with the Tg CH_3 axial conformation and the NOESY data was improved.

Refined structures

In both the Tg-axial and Tg-equatorial ensembles the *cis*-(5*R*,6*S*) lesion was positioned in the Watson–Crick orientation such that Tg NH_3 was proximate to A^{19} N1 and Tg O^4 was proximate to A^{19} N^6H (Figure 5). However, for the Tg-axial ensemble, the base pair opening at X^6•A^{19} increased such that the Tg shifted toward the major groove. For the Tg-equatorial ensemble, Tg maintained Watson–Crick positioning. Irrespective of the conformation of Tg, the complementary dA remained in the *anti* conformation about the glycosyl bond and stacked into the duplex (Figure 6). The Tg base stacked below the 5′-neighbor base G^5, while its complement A^{19} stacked below the 5′-neighbor base C^{20}. In the 3′-direction, base stacking between Tg and the G^7•C^{18} base pair was disrupted (Figure 5). Helicoidal analyses of both the axial and equatorial conformations of Tg indicated disturbances in shear, opening, stagger and stretch at the lesion (Figure 6). For the Tg CH_3 axial conformation the disturbance of the glycosyl torsion angle (χ) alleviated steric interactions between Tg CH_3 and the 5′-neighbor purine G^5. The solvent accessible surface of Tg in the duplex relative to that of a free Tg base was compared with bases A^{23}, T^9, and T^{12} (Supplementary Figure S8). Irrespective of whether the Tg CH_3 group was in the axial or equatorial conformation, Tg exhibited an increased solvent accessible surface relative to T^9 and A^{23} but was

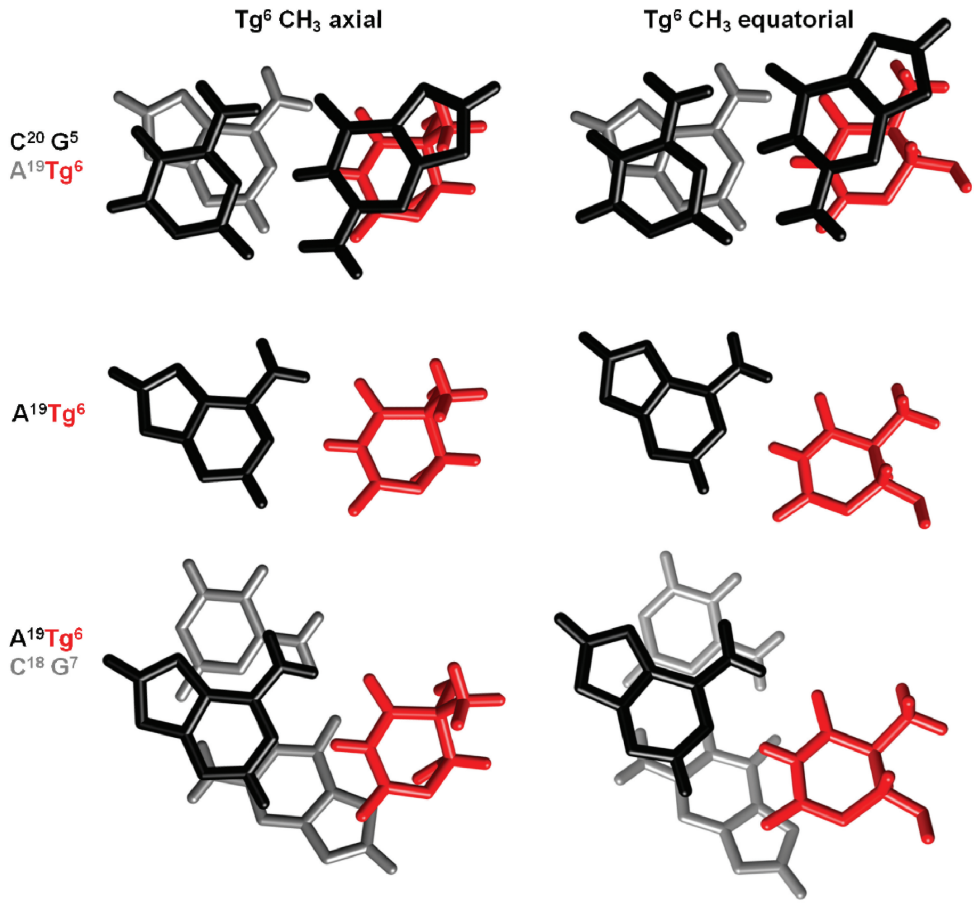

Figure 5. Base pair stacking interactions of the *cis*-(5*R*,6*S*) Tg lesion. Comparison stacking interactions in which Tg CH_3 is in the axial (PDB ID 2KH5) or equatorial (PDB ID 2KH6) conformations. The top panel shows the $G^5 \bullet C^{20}$ base pair (black) stacked above the $X^6 \bullet A^{19}$ base pair (Tg is colored red and A^{19} is colored gray). The center panel shows the orientation of the X^6 lesion (red) with respect the complementary nucleotide A^{19} (black). The bottom panel shows the $X^6 \bullet A^{19}$ base pair (Tg is colored red and A^{19} is colored black) stacked above the $G^7 \bullet C^{18}$ base pair (grey).

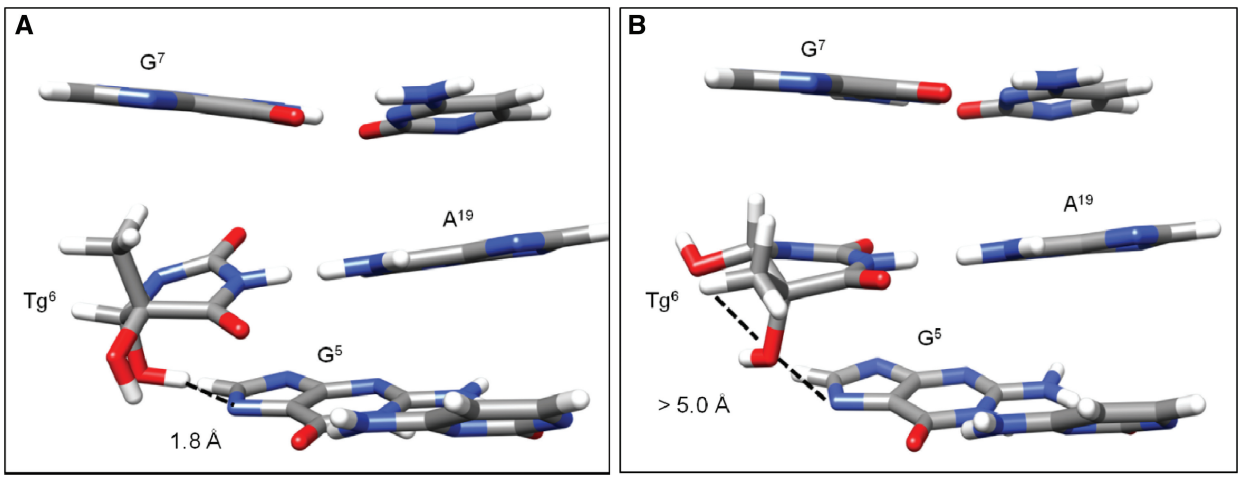

Figure 6. The *cis*-(5*R*,6*S*)Tg lesion at the $X^6 \bullet A^{19}$ base pair as viewed from the major groove showing potential hydrogen bonding interactions as predicted from analyses of rMD trajectories. (**A**) The Tg OH6 formed a hydrogen bond with G^5 N7 when Tg CH_3 was in the axial conformation (PDB ID 2KH5). (**B**) When Tg CH_3 was in the equatorial conformation Tg OH6 did not hydrogen bond with G^5 N7, however, improved hydrogen bonding was observed with Tg OH5 (PDB ID 2KH6).

not as exposed to solvent as the terminal T^{12} base. The average accessible surface area of the Tg base was 19% in the CH_3 axial structure and 18% in the CH_3 equatorial structure.

DISCUSSION

Defects in human NER are associated with the disease xeroderma pigmentosum (57,58). In human global genome NER, the XPC/HR23B complex (59–61) is the damage recognition factor. Damage-induced thermal destabilization of the helix is believed to modulate recognition of a diverse group of damages by XPC (62–66). The XPA protein is essential for NER and Yang *et al.* (67) reported that it exists as a homodimer either in the free state or as a complex with human RPA. It binds to mismatched DNA bubble substrates with or without DNA adducts, including the C8-dG adducts of AF, AAF and 1-nitropyrene, and the T[6,4]T photoproducts (68). XPA is likely involved in the verification of DNA damage (64,69). It also probably plays a role in recruitment of repair factors and stabilization of repair intermediate structures since it binds more efficiently to undamaged ds–ssDNA junctions with ssDNA branches (68), intermediate structures found in NER. In light of observations that the repair of 5*R*-Tg by DNA N-glycosylases/AP lyases is modulated by *cis–trans* epimerization (17) it was of interest to examine the 7:3 *cis*-(5*R*,6*S*): *trans*-(5*R*,6*R*) mixture of Tg epimers paired opposite adenine in the 5′-GTgG-3′ sequence (12) with regard to NER by the NER proteins of *E. coli* (18,19), and the binding of the lesion by the human NER proteins XPA and XPC/HR23B (20), and to compare these observations with the structure of the *cis*-(5*R*,6*S*) Tg lesion in this same sequence.

When placed opposite dA in the 5′-GTgG-3′ sequence the 5*R*-Tg lesion exists at 25°C as a 7:3 *cis*-(5*R*,6*S*): *trans*-(5*R*,6*R*) mixture at equilibrium; the structure of the *cis*-(5*R*,6*S*) epimer has been refined herein. That there is no disruption of sequential NOE connectivity for either the complementary strand or the modified strand (Supplementary Figure S2) supports the conclusion that the *cis*-(5*R*,6*S*) Tg lesion minimally distorts the helical backbone (12). At the X^6•A^{19} pair, both Tg and A^{19} are inserted into the helix (Figure 6). The X^6•A^{19} pair remains in a Watson–Crick type alignment in which Tg O^4 is proximate to the exocyclic amine of A^{19}, and Tg N3H is proximate to A^{19} N1 (Figure 5). Both the exchangeable Tg amine and A^{19} N^6 amine resonances protons undergo increased exchange with solvent. In the 3′-direction, stacking between the *cis*-(5*R*,6*S*) Tg^6 and the G^7•C^{18} base pair is also disrupted (Figure 6). For the X^6•A^{19} pair the *cis* (5*R*,6*S*) Tg lesion is more exposed to solvent, as compared to a Watson–Crick T•A base pair (Supplementary Figure S8). This agrees with findings in the 5′-AXA-3′ sequence when the 5*R* Tg lesion was placed opposite dA (10). Tg^6 lesion remains stacked into the duplex and it is not flipped into the major groove (Figure 6).

Nuclear magnetic resonance (NMR) does not differentiate between axial versus equatorial conformations of the Tg CH_3 group. Both are observed in the rMD calculations. The axial conformation provides a modestly improved agreement with the NOE restraints. This is consistent with the crystal structure at the nucleoside level (70). Moreover, quantum mechanical calculations of the modified base predict the axial conformation of the *cis*-(5*R*,6*S*) Tg epimer is favored (13). It was also predicted that the Tg•A pair should be stabilized by an intra-strand hydrogen bond between the Tg OH6 and the N7 position of a 3′ purine (13). Its presence is supported by analyses of the present rMD trajectories. This hydrogen bond is present when Tg CH_3 is in the axial conformation; its occupancy in the 10-ns trajectory is 46% (Supplementary Figure S5, panel D). It induces propeller twist at the lesion site, which alleviates steric interactions between the CH_3 group and the 5′-neighbor guanine. This is reflected in the perturbation of the glycosyl torsion angle χ at Tg (Supplementary Figure S5). The rMD trajectories suggest the potential for Tg OH5→G^7 N7 hydrogen bond formation when the Tg CH_3 group shifts from the axial to the equatorial conformation. This alleviates steric clash between the Tg CH_3 group and the 5′-neighbor guanine, and cannot be ruled out. However, the rMD trajectories predict only 11% occupancy of this hydrogen bond. Overall, it seems that the axial conformation of the *cis*-(5*R*,6*S*) Tg epimer is favored. The increase in longitudinal relaxation for the Tg CH_3 protons is consistent with this conclusion; in the axial conformation the Tg CH_3 group orients toward G^5. It also exhibits NOEs to G^5 protons; all are sources of longitudinal relaxation. In contrast, thymine has the CH_3 group facing into the major groove with fewer sources of longitudinal relaxation. Epimerization to the *trans*-(5*R*,6*R*) Tg lesion, for which the equatorial conformation of the Tg CH_3 group is favored by 4 kcal/mol (13), probably represents the more favorable mechanism for alleviating steric strain (12). Consistent with this conclusion, in the structure of the RB69 polymerase involving a template containing the *cis*-(5*R*,6*S*) Tg lesion and an incoming dATP, the Tg CH_3 group is in the axial conformation, despite hindering stacking of the adjacent 5′-template guanine (71). Bolton and co-workers (11) reported that a disordered structure resulted when 5*R*-Tg was placed into a duplex containing the 5′-G<u>Tg</u>C-3′ sequence. This suggests that formation of an intra-strand hydrogen between the Tg C6 OH and the N7 position of a 3′ purine (13) is important in stabilizing the *cis*-(5*R*,6*S*) Tg lesion in duplex DNA.

The observation that the K_d values of XPC/HR23B from either the 5*R*-Tg- (~18 nM) or AAF-DNA substrates (~27 nM) are lower than those from XPA is consistent with the proposed role of XPC/HR23B as the damage recognition factor in human genomic NER (64,69). In comparison, XPC/HR23B binds to cisplatin 1,3-intrastrand adducts or 6-nt lengths of mispaired DNA with a K_d of 1–3 nM (64). The recognition of the AAF-damaged DNA by XPC/HR23B has been attributed to the adduct's inability to base pair efficiently with cytosine (72), and an emerging consensus posits that

disruption of normal base pairing and the resulting destabilization of the helix, rather than the recognition of helical distortion by bulky lesions, governs the affinity of XPC/HR23B binding (73). It should be noted, however, that while 5*R*-Tg can be recognized by XPC/HR23B and XPA, the efficiency of incision of this site-specific lesion by the human NER system remains to be determined.

From studies of the yeast XPC orthologue Rad4 bound to DNA containing a cyclobutane pyrimidine dimer, Min and Pavletch (74) concluded that damage recognized by Rad4 destabilizes the helix and facilitates the flipping out of two base pairs by the protein. The present data are consistent with this model. The presence of 5*R*-Tg in the duplex perturbs the 5′-neighbor base pair G^5•C^{20}, in addition to the damaged base pair X^6•A^{19}. As indicated in Figure 5, the imino resonance of base pair G^5•C^{20} broadens due to solvent exchange. In fact, it disappears from the ^{1}H NMR spectrum ~35°C lower in the 5*R*-Tg modified DNA as compared to the unmodified duplex (12).

This destabilization of the two base pairs by the cis-(5*R*,6*S*) epimer may lower the activation barrier with respect to flipping both base pairs out of the helix, enabling XPC/HR23B to recognize the 5*R* Tg lesion prior to the recruitment of XPA. Based upon MD simulations of the Dickerson-Drew 5*R*-Tg-modified dodecamer d(CGCGAATgTCGCG)$_2$, both Miller *et al.* (75) and Miaskiewicz *et al.* (76) also concluded that Tg weakened Watson–Crick hydrogen bonds of the 5′-neighbor base pair. The increase in transverse relaxation for Tg CH_3 as compared to unmodified thymine CH_3 protons is attributed to the puckering of the Tg six-member ring. However, increased backbone and sugar motions in tandem with the puckering of the Tg ring cannot be excluded.

The 5*R*-Tg lesion is also a substrate for base excision repair in *E. coli* and in mammalian cells (77). In *E. coli*, repair of Tg is initiated by endonuclease III (Nth) (78) and endonuclease VIII (Nei) (79). Yeast (80), mammalian (81,82) and human orthologs (83–85) of Nth have been characterized. Likewise, human orthologs of Nei have been characterized (86,87). The human hNTH1 exhibits a 13:1 preference for excising the 5*R* versus the 5*S* epimers, whereas hNEIL1 (86,88) shows a 1.5:1 preference for excising the 5*R* versus the 5*S* epimers (89). Similar observations have been made for prokaryotic, yeast and murine glycosylases (90). Ocampa-Hafalla *et al.* (17) showed that the repair of Tg by DNA N-glycosylases/AP lyases is modulated by the *cis–trans* epimerization of these two sets of diastereomers and that repair of 5*R* Tg by hNEIL1 depends upon the opposing base, with Tg•G pairs being excised much more rapidly than Tg•A pairs. Significantly, when 5-methyl cytosine is oxidatively damaged, forming 5-methycytosine glycol, hydrolytic deamination yields Tg mismatched with dG in (3). Computational studies suggest that substrates for hNEIL1 possess in common a pyrimidine-like ring and hydrogen bond donor-acceptor properties, allowing them to be accommodated within the enzyme's binding pocket (91). Based upon structural data for the 5*R*-Tg lesion in a T•G mismatch, we suggested that the wobble orientation of the *cis*-(5*R*,6*S*) Tg base in the Tg•G pair shifts it toward the major groove, reflected in an increased solvent accessible surface and reduced barrier for intrinsic breathing of the lesion (14). While the Tg•A structure also shows an increased solvent accessible surface area, it differs from the Tg•G pair in that an efficient hydrogen bond between Tg OH6→G^7 N7 is possible; this may be sufficient to reduce the barrier toward base-flipping of the Tg lesion into the active site pocket of the glycosylase.

In summary, in the 5′-GTG-3′ sequence, 5*R*-Tg, paired with dA, is a good binding substrate for the NER proteins from *E. Coli* and humans, corroborating earlier reports (18–20). It is a better substrate of the human NER proteins XPA and XPC/HR23B in comparison to the C8 dG adduct of AAF. The structure of the *cis*-(5*R*,6*S*) Tg lesion in this same sequence is consistent with the repair data in that the lesion causes destabilization of the 5′-neighboring GC base pair, in addition to an increase in the solvent accessible area of Tg. It is conceivable that these thermodynamic perturbations of two base pairs contribute toward efficient recognition and NER of the 5*R*-Tg lesion.

ACCESSION NUMBERS

PDB ID 2KH5, PDB ID 2KH6.

SUPPLEMENTARY DATA

Supplementary Data are available at NAR Online.

ACKNOWLEDGEMENTS

Dr Markus Voehler and Dr Don Stec assisted with NMR spectroscopy. Dr Nicholas Uylanov and Dr Jarrod A. Smith assisted with structural refinement. Professor D. A. Johnson, ETSU, provided the human serum albumin. Drs Thomas M. and Constance M. Harris provided constructive comments.

FUNDING

National Institutes of Health Grants R01 CA-055678 and P30 ES-000267 (to M.P.S.) and R01 ES-013324 (to A.K.B). Funding for open access charge: National Institutes of Health Grant R01 CA-55678.

Conflict of interest statement. None declared.

REFERENCES

1. Teoule,R., Bonicel,A., Bert,C., Cadet,J. and Polverelli,M. (1974) Identification of radioproducts resulting from the breakage of thymine moiety by gamma irradiation of *E.* coli DNA in an aerated aqueous solution. *Radiat. Res.*, **57**, 46–58.
2. Frenkel,K., Goldstein,M.S. and Teebor,G.W. (1981) Identification of the cis-thymine glycol moiety in chemically oxidized and gamma-irradiated deoxyribonucleic acid by high-pressure liquid chromatography analysis. *Biochemistry*, **20**, 7566–7571.
3. Zuo,S., Boorstein,R.J. and Teebor,G.W. (1995) Oxidative damage to 5-methylcytosine in DNA. *Nucleic Acids Res.*, **23**, 3239–3243.

4. Pfeifer,G.P. (2000) p53 mutational spectra and the role of methylated CpG sequences. *Mutat. Res.*, **450**, 155–166.
5. Vaishnav,Y., Holwitt,E., Swenberg,C., Lee,H.C. and Kan,L.S. (1991) Synthesis and characterization of stereoisomers of 5,6-dihydro-5,6-dihydroxy-thymidine. *J. Biomol. Struct. Dyn.*, **8**, 935–951.
6. Lustig,M.J., Cadet,J., Boorstein,R.J. and Teebor,G.W. (1992) Synthesis of the diastereomers of thymidine glycol, determination of concentrations and rates of interconversion of their cis-trans epimers at equilibrium and demonstration of differential alkali lability within DNA. *Nucleic Acids Res.*, **20**, 4839–4845.
7. Wang,Y. (2002) HPLC isolation and mass spectrometric characterization of two isomers of thymine glycols in oligodeoxynucleotides. *Chem. Res. Toxicol.*, **15**, 671–676.
8. Cathcart,R., Schwiers,E., Saul,R.L. and Ames,B.N. (1984) Thymine glycol and thymidine glycol in human and rat urine: a possible assay for oxidative DNA damage. *Proc. Natl Acad. Sci. USA*, **81**, 5633–5637.
9. Adelman,R., Saul,R.L. and Ames,B.N. (1988) Oxidative damage to DNA: relation to species metabolic rate and life span. *Proc. Natl Acad. Sci. USA*, **85**, 2706–2708.
10. Kung,H.C. and Bolton,P.H. (1997) Structure of a duplex DNA containing a thymine glycol residue in solution. *J. Biol. Chem.*, **272**, 9227–9236.
11. Kao,J.Y., Goljer,I., Phan,T.A. and Bolton,P.H. (1993) Characterization of the effects of a thymine glycol residue on the structure, dynamics, and stability of duplex DNA by NMR. *J. Biol. Chem.*, **268**, 17787–17793.
12. Brown,K.L., Adams,T., Jasti,V.P., Basu,A.K. and Stone,M.P. (2008) Interconversion of the *cis*-5R,6*S*- and *trans*-5*R*,6*R*-thymine glycol lesions in duplex DNA. *J. Am. Chem. Soc.*, **129**, 11701–11710.
13. Clark,J.M., Pattabiraman,N., Jarvis,W. and Beardsley,G.P. (1987) Modeling and molecular mechanical studies of the cis-thymine glycol radiation damage lesion in DNA. *Biochemistry*, **26**, 5404–5409.
14. Brown,K.L., Basu,A.K. and Stone,M.P. The cis-(5R,6S)-thymine glycol lesion occupies the wobble position when mismatched with dG in DNA. *Biochemistry*, **48**, 9722–9733.
15. Ide,H., Kow,Y.W. and Wallace,S.S. (1985) Thymine glycols and urea residues in M13 DNA constitute replicative blocks *in vitro*. *Nucleic Acids Res.*, **13**, 8035–8052.
16. Clark,J.M. and Beardsley,G.P. (1986) Thymine glycol lesions terminate chain elongation by DNA polymerase I *in vitro*. *Nucleic Acids Res.*, **14**, 737–749.
17. Ocampo-Hafalla,M.T., Altamirano,A., Basu,A.K., Chan,M.K., Ocampo,J.E., Cummings,A. Jr, Boorstein,R.J., Cunningham,R.P. and Teebor,G.W. (2006) Repair of thymine glycol by hNth1 and hNeil1 is modulated by base pairing and *cis*-trans epimerization. *DNA Repair (Amst)*, **5**, 444–454.
18. Lin,J.J. and Sancar,A. (1989) A new mechanism for repairing oxidative damage to DNA: (A)BC excinuclease removes AP sites and thymine glycols from DNA. *Biochemistry*, **28**, 7979–7984.
19. Kow,Y.W., Wallace,S.S. and Van Houten,B. (1990) UvrABC nuclease complex repairs thymine glycol, an oxidative DNA base damage. *Mutat. Res.*, **235**, 147–156.
20. Reardon,J.T., Bessho,T., Kung,H.C., Bolton,P.H. and Sancar,A. (1997) In vitro repair of oxidative DNA damage by human nucleotide excision repair system: possible explanation for neurodegeneration in xeroderma pigmentosum patients. *Proc. Natl Acad. Sci. USA*, **94**, 9463–9468.
21. Yang,Z., Colis,L.C., Basu,A.K. and Zou,Y. (2005) Recognition and incision of gamma-radiation-induced cross-linked guanine-thymine tandem lesion G[8,5-Me]T by UvrABC nuclease. *Chem. Res. Toxicol.*, **18**, 1339–1346.
22. Liu,Y., Liu,Y., Yang,Z., Utzat,C., Wang,G., Basu,A.K. and Zou,Y. (2005) Cooperative interaction of human XPA stabilizes and enhances specific binding of XPA to DNA damage. *Biochemistry*, **44**, 7361–7368.
23. Piotto,M., Saudek,V. and Sklenar,V. (1992) Gradient-tailored excitation for single-quantum NMR spectroscopy of aqueous solutions. *J. Biomol. NMR*, **2**, 661–665.
24. Carr,H.Y. and Purcell,E.M. (1954) Effects of diffusion on free precession in nuclear magnetic resonance experiments. *Phys. Rev.*, **94**, 630.
25. Vold,R.L., Waugh,J.S., Klein,M.P. and Phelps,D.E. (1968) Measurement of spin relaxation in complex systems. *J. Chem. Phys.*, **48**, 3831–3832.
26. Goddard,T.D. and Kneller,D.G. (2006) SPARKY v. 3.113. University of California, San Francisco.
27. Keepers,J.W. and James,T.L. (1984) A theoretical study of distance determinations from NMR – two-dimensional nuclear Overhauser effect spectra. *J. Magn. Reson.*, **57**, 404–426.
28. James,T.L. (1991) Relaxation matrix analysis of two-dimensional nuclear Overhauser effect spectra. *Curr. Opin. Struct. Biol.*, **1**, 1042–1053.
29. Borgias,B.A. and James,T.L. (1989) Two-dimensional nuclear Overhauser effect: complete relaxation matrix analysis. *Methods Enzymol.*, **176**, 169–183.
30. Borgias,B.A. and James,T.L. (1990) MARDIGRAS – a procedure for matrix analysis of relaxation for discerning geometry of an aqueous structure. *J. Magn. Reson.*, **87**, 475–487.
31. Liu,H., Spielmann,H.P., Ulyanov,N.B., Wemmer,D.E. and James,T.L. (1995) Interproton distance bounds from 2D NOE intensities: effect of experimental noise and peak integration errors. *J. Biomol. NMR*, **6**, 390–402.
32. Delaglio,F., Wu,Z. and Bax,A. (2001) Measurement of homonuclear proton couplings from regular 2D COSY spectra. *J. Magn. Reson.*, **149**, 276–281.
33. Van De Ven,F.J.M. and Hilbers,C.W. (1988) Nucleic acids and nuclear magnetic resonance. *Eur. J. Biochem.*, **178**, 1–38.
34. van Wijk,J., Huckriede,B.D., Ippel,J.H. and Altona,C. (1992) Furanose sugar conformations in DNA from NMR coupling constants. *Methods Enzymol.*, **211**, 286–306.
35. Frisch,M.J., Trucks,G.W., Schlegel,H.B., Scuseria,G.E., Robb,M.A., Cheeseman,J.R., Montgomery,J.A., Vreven,T., Kudin,K.N., Burant,J.C. *et al.* (2004) GAUSSIAN 03. Gaussian, Inc., Wallingford, CT.
36. Case,D.A., Cheatham,T.E. III, Darden,T., Gohlke,H., Luo,R., Merz,K.M. Jr, Onufriev,A., Simmerling,C., Wang,B. and Woods,R.J. (2005) The AMBER biomolecular simulation programs. *J. Comput. Chem.*, **26**, 1668–1688.
37. Macke,T. and Case,D.A. (1998) In Leontes,N.B. and SantaLucia,J. Jr (eds), *Molecular Modeling of Nucleic Acids*, Vol. 682. American Chemical Society, Washington, D.C.
38. Wang,J.M., Cieplak,P. and Kollman,P.A. (2000) How well does a restrained electrostatic potential (RESP) model perform in calculating conformational energies of organic and biological molecules? *J. Comput. Chem.*, **21**, 1049–1074.
39. Clore,G.M., Brunger,A.T., Karplus,M. and Gronenborn,A.M. (1986) Application of molecular dynamics with interproton distance restraints to three-dimensional protein structure determination. *J. Mol. Biol.*, **191**, 523–551.
40. Tsui,V. and Case,D.A. (2000) Theory and applications of the generalized Born solvation model in macromolecular simulations. *Biopolymers*, **56**, 275–291.
41. Bashford,D. and Case,D.A. (2000) Generalized Born models of macromolecular solvation effects. *Annu. Rev. Phys. Chem.*, **51**, 129–152.
42. Berendsen,H.J.C., Postma,J.P.M., van Gunsteren,W.F., DiNola,A. and Haak,J.R. (1984) Molecular dynamics with coupling to an external bath. *J. Phys. Chem.*, **81**, 3684–3690.
43. Loncharich,R.J., Brooks,B.R. and Pastor,R.W. (1992) Langevin dynamics of peptides: the frictional dependence of isomerization rates of N-acetylalanyl-N′-methylamide. *Biopolymers*, **32**, 523–535.
44. Izaguirre,J.A., Catarello,D.P., Wozniak,J.M. and Skeel,R.D. (2001) Langevin stabilization of molecular dynamics. *J. Chem. Phys.*, **114**, 2090–2098.
45. Essmann,U., Perera,L., Berkowitz,M.L., Darden,T., Lee,H. and Pedersen,L.G. (1995) A smooth particle mesh Ewald method. *J. Chem. Phys.*, **103**, 8577–8593.
46. Ryckaert,J.P., Ciccotti,G. and Berendsen,H.J.C. (1977) Numerical integration of cartesian equations of motion of a system with constraints: molecular dynamics of N-alkanes. *J. Comput. Phys.*, **23**, 327–341.

47. Lavery,R. and Sklenar,H. (1988) The definition of generalized helicoidal parameters and of axis curvature for irregular nucleic-acids. *J. Biomol. Struct. Dyn.*, **6**, 63–91.
48. Ravishanker,G., Swaminathan,S., Beveridge,D.L., Lavery,R. and Sklenar,H. (1989) Conformational and helicoidal analysis of 30 ps of molecular-dynamics on the d(CGCGAATTCGCG) double helix – curves, dials and windows. *J. Biomol. Struct. Dyn.*, **6**, 669–699.
49. Pettersen,E.F., Goddard,T.D., Huang,C.C., Couch,G.S., Greenblatt,D.M., Meng,E.C. and Ferrin,T.E. (2004) UCSF chimera: a visualization system for exploratory research and analysis. *J. Comput. Chem.*, **25**, 1605–1612.
50. Sanner,M.F., Olson,A.J. and Spehner,J.C. (1996) Reduced surface: an efficient way to compute molecular surfaces. *Biopolymers*, **38**, 305–320.
51. Mekhovich,O., Tang,M. and Romano,L.J. (1998) Rate of incision of N-acetyl-2-aminofluorene and N-2-aminofluorene adducts by UvrABC nuclease is adduct- and sequence-specific: comparison of the rates of UvrABC nuclease incision and protein–DNA complex formation. *Biochemistry*, **37**, 571–579.
52. Zou,Y., Shell,S.M., Utzat,C.D., Luo,C., Yang,Z., Geacintov,N.E. and Basu,A.K. (2003) Effects of DNA adduct structure and sequence context on strand opening of repair intermediates and incision by UvrABC nuclease. *Biochemistry*, **42**, 12654–12661.
53. Meneni,S.R., D'Mello,R., Norigian,G., Baker,G., Gao,L., Chiarelli,M.P. and Cho,B.P. (2006) Sequence effects of aminofluorene-modified DNA duplexes: thermodynamic and circular dichroism properties. *Nucleic Acids Res*, **34**, 755–763.
54. Reid,B.R. (1987) Sequence-specific assignments and their use in NMR studies of DNA structure. *Q. Rev. Biophys.*, **20**, 2–28.
55. Patel,D.J., Shapiro,L. and Hare,D. (1987) DNA and RNA: NMR studies of conformations and dynamics in solution. *Q. Rev. Biophys.*, **20**, 35–112.
56. Boelens,R., Scheek,R.M., Dijkstra,K. and Kaptein,R. (1985) Sequential assignment of imino- and amino-proton resonances in ^{1}H NMR spectra of oligonucleotides by two-dimensional NMR spectroscopy. Application to a lac operator fragment. *J. Magn. Reson.*, **62**, 378–386.
57. Cleaver,J.E. (2005) Cancer in xeroderma pigmentosum and related disorders of DNA repair. *Nat. Rev. Cancer*, **5**, 564–573.
58. Cleaver,J.E. (2008) Historical aspects of xeroderma pigmentosum and nucleotide excision repair. *Adv. Exp. Med. Biol.*, **637**, 1–9.
59. Legerski,R. and Peterson,C. (1992) Expression cloning of a human DNA repair gene involved in xeroderma pigmentosum group C. *Nature*, **359**, 70–73.
60. Masutani,C., Sugasawa,K., Yanagisawa,J., Sonoyama,T., Ui,M., Enomoto,T., Takio,K., Tanaka,K., van der Spek,P.J., Bootsma,D. *et al.* (1994) Purification and cloning of a nucleotide excision repair complex involving the xeroderma pigmentosum group C protein and a human homologue of yeast RAD23. *EMBO J.*, **13**, 1831–1843.
61. Volker,M., Mone,M.J., Karmakar,P., van Hoffen,A., Schul,W., Vermeulen,W., Hoeijmakers,J.H., van Driel,R., van Zeeland,A.A. and Mullenders,L.H. (2001) Sequential assembly of the nucleotide excision repair factors in vivo. *Mol. Cell*, **8**, 213–224.
62. Gunz,D., Hess,M.T. and Naegeli,H. (1996) Recognition of DNA adducts by human nucleotide excision repair. Evidence for a thermodynamic probing mechanism. *J. Biol. Chem.*, **271**, 25089–25098.
63. Buterin,T., Hess,M.T., Luneva,N., Geacintov,N.E., Amin,S., Kroth,H., Seidel,A. and Naegeli,H. (2000) Unrepaired fjord region polycyclic aromatic hydrocarbon-DNA adducts in ras codon 61 mutational hot spots. *Cancer Res.*, **60**, 1849–1856.
64. Hey,T., Lipps,G., Sugasawa,K., Iwai,S., Hanaoka,F. and Krauss,G. (2002) The XPC-HR23B complex displays high affinity and specificity for damaged DNA in a true-equilibrium fluorescence assay. *Biochemistry*, **41**, 6583–6587.
65. Dip,R., Camenisch,U. and Naegeli,H. (2004) Mechanisms of DNA damage recognition and strand discrimination in human nucleotide excision repair. *DNA Repair (Amst)*, **3**, 1409–423.
66. Buterin,T., Meyer,C., Giese,B. and Naegeli,H. (2005) DNA quality control by conformational readout on the undamaged strand of the double helix. *Chem. Biol.*, **12**, 913–922.
67. Yang,Z.G., Liu,Y., Mao,L.Y., Zhang,J.T. and Zou,Y. (2002) Dimerization of human XPA and formation of XPA2-RPA protein complex. *Biochemistry*, **41**, 13012–13020.
68. Yang,Z., Roginskaya,M., Colis,L.C., Basu,A.K., Shell,S.M., Liu,Y., Musich,P.R., Harris,C.M., Harris,T.M. and Zou,Y. (2006) Specific and efficient binding of xeroderma pigmentosum complementation group A to double-strand/single-strand DNA junctions with 3′- and/or 5′-ssDNA branches. *Biochemistry*, **45**, 15921–15930.
69. Riedl,T., Hanaoka,F. and Egly,J.M. (2003) The comings and goings of nucleotide excision repair factors on damaged DNA. *EMBO J.*, **22**, 5293–5303.
70. Hruska,F.E., Sebastian,R., Grand,A., Voituriez,L. and Cadet,J. (1987) Characterization of a gamma-radiation-induced decomposition product of thymidine. Crystal and molecular structure of the (-)cis(5R,6S) thymidine glycol. *Can. J. Chem.*, **65**, 2618–2623.
71. Aller,P., Rould,M.A., Hogg,M., Wallace,S.S. and Doublie,S. (2007) A structural rationale for stalling of a replicative DNA polymerase at the most common oxidative thymine lesion, thymine glycol. *Proc. Natl Acad. Sci. USA*, **104**, 814–818.
72. O'Handley,S.F., Sanford,D.G., Xu,R., Lester,C.C., Hingerty,B.E., Broyde,S. and Krugh,T.R. (1993) Structural characterization of an N-acetyl-2-aminofluorene (AAF) modified DNA oligomer by NMR, energy minimization, and molecular dynamics. *Biochemistry*, **32**, 2481–2497.
73. Sugasawa,K., Shimizu,Y., Iwai,S. and Hanaoka,F. (2002) A molecular mechanism for DNA damage recognition by the xeroderma pigmentosum group C protein complex. *DNA Repair (Amst)*, **1**, 95–107.
74. Min,J.H. and Pavletich,N.P. (2007) Recognition of DNA damage by the Rad4 nucleotide excision repair protein. *Nature*, **449**, 570–575.
75. Miller,J., Miaskiewicz,K. and Osman,R. (1994) Structure–function studies of DNA damage using ab initio quantum mechanics and molecular dynamics simulation. *Ann. NY Acad. Sci.*, **726**, 71–91.
76. Miaskiewicz,K., Miller,J., Ornstein,R. and Osman,R. (1995) Molecular dynamics simulations of the effects of ring-saturated thymine lesions on DNA structure. *Biopolymers*, **35**, 113–124.
77. Hazra,T.K., Das,A., Das,S., Choudhury,S., Kow,Y.W. and Roy,R. (2007) Oxidative DNA damage repair in mammalian cells: a new perspective. *DNA Repair (Amst)*, **6**, 470–480.
78. Weiss,B. and Cunningham,R.P. (1985) Genetic mapping of Nth, a gene affecting endonuclease III (thymine glycol-DNA glycosylase) in *Escherichia coli* K-12. *J. Bacteriol.*, **162**, 607–610.
79. Jiang,D., Hatahet,Z., Melamede,R.J., Kow,Y.W. and Wallace,S.S. (1997) Characterization of *Escherichia coli* endonuclease VIII. *J. Biol. Chem.*, **272**, 32230–32239.
80. Roldan-Arjona,T., Anselmino,C. and Lindahl,T. (1996) Molecular cloning and functional analysis of a *Schizosaccharomyces pombe* homologue of *Escherichia coli* endonuclease III. *Nucleic Acids Res.*, **24**, 3307–3312.
81. Hilbert,T.P., Boorstein,R.J., Kung,H.C., Bolton,P.H., Xing,D., Cunningham,R.P. and Teebor,G.W. (1996) Purification of a mammalian homologue of *Escherichia coli* endonuclease III: identification of a bovine pyrimidine hydrate-thymine glycol DNAse/AP lyase by irreversible cross linking to a thymine glycol-containing oligoxynucleotide. *Biochemistry*, **35**, 2505–2511.
82. Sarker,A.H., Ikeda,S., Nakano,H., Terato,H., Ide,H., Imai,K., Akiyama,K., Tsutsui,K., Bo,Z., Kubo,K. *et al.* (1998) Cloning and characterization of a mouse homologue (mNthl1) of *Escherichia coli* endonuclease III. *J. Mol. Biol.*, **282**, 761–774.
83. Hilbert,T.P., Chaung,W., Boorstein,R.J., Cunningham,R.P. and Teebor,G.W. (1997) Cloning and expression of the cDNA encoding the human homologue of the DNA repair enzyme, *Escherichia coli* endonuclease III. *J. Biol. Chem.*, **272**, 6733–6740.
84. Aspinwall,R., Rothwell,D.G., Roldan-Arjona,T., Anselmino,C., Ward,C.J., Cheadle,J.P., Sampson,J.R., Lindahl,T., Harris,P.C. and Hickson,I.D. (1997) Cloning and characterization of a functional human homolog of *Escherichia coli* endonuclease III. *Proc. Natl Acad. Sci. USA*, **94**, 109–114.
85. Ikeda,S., Biswas,T., Roy,R., Izumi,T., Boldogh,I., Kurosky,A., Sarker,A.H., Seki,S. and Mitra,S. (1998) Purification and characterization of human NTH1, a homolog of *Escherichia coli*

endonuclease III. Direct identification of Lys-212 as the active nucleophilic residue. *J. Biol. Chem.*, **273**, 21585–21593.
86. Hazra,T.K., Izumi,T., Boldogh,I., Imhoff,B., Kow,Y.W., Jaruga,P., Dizdaroglu,M. and Mitra,S. (2002) Identification and characterization of a human DNA glycosylase for repair of modified bases in oxidatively damaged DNA. *Proc. Natl Acad. Sci. USA*, **99**, 3523–3528.
87. Hazra,T.K., Kow,Y.W., Hatahet,Z., Imhoff,B., Boldogh,I., Mokkapati,S.K., Mitra,S. and Izumi,T. (2002) Identification and characterization of a novel human DNA glycosylase for repair of cytosine-derived lesions. *J. Biol. Chem.*, **277**, 30417–30420.
88. Bandaru,V., Sunkara,S., Wallace,S.S. and Bond,J.P. (2002) A novel human DNA glycosylase that removes oxidative DNA damage and is homologous to *Escherichia coli* endonuclease VIII. *DNA Repair (Amst)*, **1**, 517–529.
89. Katafuchi,A., Nakano,T., Masaoka,A., Terato,H., Iwai,S., Hanaoka,F. and Ide,H. (2004) Differential specificity of human and *Escherichia coli* endonuclease III and VIII homologues for oxidative base lesions. *J. Biol. Chem.*, **279**, 14464–14471.
90. Miller,H., Fernandes,A.S., Zaika,E., McTigue,M.M., Torres,M.C., Wente,M., Iden,C.R. and Grollman,A.P. (2004) Stereoselective excision of thymine glycol from oxidatively damaged DNA. *Nucleic Acids Res.*, **32**, 338–345.
91. Jia,L., Shafirovich,V., Geacintov,N.E. and Broyde,S. (2007) Lesion specificity in the base excision repair enzyme hNeil1: modeling and dynamics studies. *Biochemistry*, **46**, 5305–5314.